

Chemical-Looping Reforming of Methane Using Iron Based Oxygen Carrier Modified with Low Content Nickel

Guoqiang Wei, Fang He,* Zhen Huang, Kun Zhao, Anqing Zheng, and Haibin Li

CAS Key Laboratory of Renewable Energy, Guangzhou Institute of Energy Conversion, Chinese Academy of Sciences, Guangzhou, Guangdong 510640, China

$\text{Fe}_2\text{O}_3/\text{Al}_2\text{O}_3$ and $\text{Fe}_2\text{O}_3/\text{Al}_2\text{O}_3$ modified by low content of Ni (below 2% in weight) oxygen carriers were prepared by mechanical mixing and impregnation method. The synthesized oxygen carriers were characterized by means of X-ray diffraction (XRD), X-ray fluorescence (XRF), scanning electron microscopy (SEM), BET-surface area and temperature programmed reduction (TPR). Besides, redox cyclic reactivity and the performance of chemical looping reforming of methane of the oxygen carriers were studied in a thermal gravimetric analysis (TGA) and fixed bed at 850 °C. It was observed that the redox reactivity of the oxygen carriers is improved by Ni addition because synergic effect may occur between NiO and $\text{Fe}_2\text{O}_3/\text{Al}_2\text{O}_3$ to form NiFe_2O_4 and NiAl_2O_4 spinel phases. However, the improvement was not apparent as Ni addition reached 1 wt% or more because more nickel loaded resulted in methane decomposition into H_2 and carbon leading to carbon deposition. The SEM and BET analysis showed that NiFe_2O_4 and NiAl_2O_4 particles dispersed into the pores of the $\text{Fe}_2\text{O}_3/\text{Al}_2\text{O}_3$ particles in the course of preparation. In addition, the resistance to sintering of the modified samples increased with the Ni addition increasing. The results of successive redox cycles showed that the Ni modified $\text{Fe}_2\text{O}_3/\text{Al}_2\text{O}_3$ oxygen carriers have good regenerability. With integration of reactivity and carbon deposition, the content 1.04 wt% of nickel doping was an optimal amount in the three modified samples.

Keywords methane, chemical-looping reforming, chemical-looping reforming, oxygen carrier, iron, low content, nickel

Introduction

Synthesis gas, which is mainly composed of H_2 and CO, can be used to produce ammonia, methanol, hydrogen and other chemical products. At present, steam or CO_2 reforming of natural gas was reacted in reactor tubes packed with catalyst and it has been developed into a large-scale production. The chemical reactions of the above-mentioned routes are shown as follows:^[1]

Steam reforming:



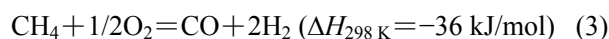
CO_2 reforming:^[2]



These two reactions, which are highly endothermic reactions, consume a large amount of energy, and the H_2/CO ratio is unsuitable for the Fischer-Tropsch and methanol syntheses in which the desired H_2/CO ratio is 2. In contrast to the two methods above mentioned, another methane reforming approach, *i.e.* partial oxidation of methane (POM), was proposed with a mild exothermic reaction and a H_2/CO ratio of 2 according to the Eq.

(3).

POM to synthesis gas:



An economic analysis^[3] suggests that the POM to synthesis gas requires half of the capital investment in the gas-to-liquid process compared to the typical steam reforming for the reason that the significant capital cost of building and running the oxygen plant will be avoided, if lattice oxygen of solid oxygen carriers instead of pure oxygen is used as the oxygen source of methane oxidation.^[4,5] The Chemical-looping reforming (CLR) process was a new technology for synthesis gas (H_2 and CO) production from natural gas and light hydrocarbons by using lattice oxygen instead of molecular oxygen, which was a POM process, essentially. This new technology was presented by Mattisson and Lyngfelt.^[6] The most important advantage of CLR is to produce synthesis gas, which is not diluted with N_2 . Besides, Since the heat transfer occurs directly between gas and oxygen carriers, it is more effective to reduce the size of the reformer, the CLR is economic than conventional technology.^[7-9]

* E-mail: hefang@ms.giec.ac.cn; Tel.: 0086-020-87057721; Fax: 0086-020-87057737

Received August 19, 2014; accepted November 4, 2014; published online December 9, 2014.

Based on the principle of chemical-looping combustion (CLC),^[10] the CLR has a different target product, which is synthesis gas rather than heat in CLC.^[11] Similar to CLC, the CLR system consists of two separate reactors, an air reactor (AR) and a fuel reactor (FR), as shown in Figure 1. As a carrier of oxygen and heat, the particles of oxygen carrier play an important role in the CLR process. The properties of oxygen carrier are critical and the following are desired: high reactivity, high oxygen transport capacity and high resistance against mechanical, thermal stress.

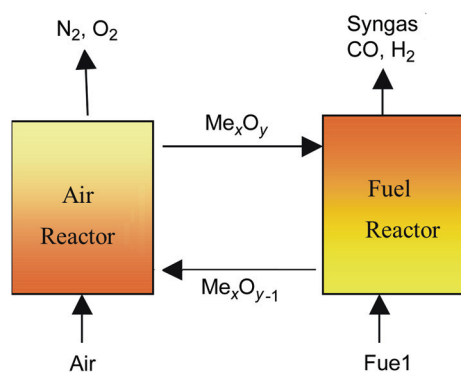


Figure 1 Schematic description of chemical-looping reforming.

Oxides of some metals, such as Ni, Fe, Co, Cu, and Mn have been intensively tested to be used as oxygen carriers for CLR.^[12–15] Generally, Ni-based oxygen carriers are demonstrated a higher redox rate than other metals. While, its toxicity to the environment needs attention if much more Ni-based oxygen carriers are used.^[16] Meanwhile, the CuO oxygen carriers were also found to have very favorable reactivity giving complete fuel combustion to CO₂ and H₂O.^[17,18] However, Cu-based oxygen carriers are limited to use at a relatively low temperature due to the low melting point of Cu.^[19,20] Iron oxide is an attractive oxygen carrier for the application of CLR of methane because of its abundance, high melting point and low price, but it is often restricted for the lower reactivity rate and oxygen transport capacity.^[21] Mixed-metal oxides by combining different materials may create synergistic effects giving good reactivity and selectivity,^[22] as well as enhance the dispersion of active metals.^[23–26] Therefore, mixed-metal oxides could be a way to develop novel oxygen carriers with better reactivity. Various combining oxygen carriers such as Fe₂O₃-NiO, Fe₂O₃-Mn₃O₄, NiO-MgAl₂O₄, Fe₂O₃-MgAl₂O₄, and CeO₂-Fe₂O₃, which reacted with CH₄, coal and biomass were studied widely in fixed or fluidized bed reactors, indicating better reactivity, anti-sintering and carbon deposition than single oxide.^[27–31] Also, Perovskite-type mixed metal oxides were examined in the chemical looping reforming of methane for their high oxygen mobility in the bulk and thermal stability,^[32,33] however, there is a limitation of mechanical properties on its application for long time. Usually, an inert binder, such as Al₂O₃, SiO₂, TiO₂ and

ZrO, was employed as support in the oxygen carriers to obtain a better reactivity, durability, and fluidizability of the oxygen carrier particles.

Although a number of researches have been conducted on the reactivity of Fe₂O₃ and NiO with CH₄,^[34–36] studies related to the reactivity of iron oxide combining with low nickel content are still scarce. However, the low nickel content in modified oxygen carriers is of significant practical importance in applications such as reduction of carbon deposition, environment pollution and reforming cost as well as improving reactivity of syngas production. Rydén *et al.*^[31] evaluated the reactivity of Fe₂O₃/MgAl₂O₄ with 1% and 10% NiO/MgAl₂O₄ in CLC or CLR of methane in a fixed-bed quartz reactor at 900 °C and the results showed that adding 1% NiO/MgAl₂O₄ into the Fe₂O₃/MgAl₂O₄ particles had no positive effects on CLC but increased both reactivity and selectivity of methane reforming. However, other different contents of NiO added into the Fe₂O₃/Al₂O₃ particles were not further examined.

Pans *et al.*^[24] also used chemically and physically mixed iron and nickel oxides as oxygen carriers for gas combustion in a CLC process. Different bimetallic Fe-Ni-based OCs had been prepared and evaluated in a TGA, a batch fluidized bed reactor, and a continuous CLC unit in order to analyze the effect of NiO content on the CLC performance when CH₄ was used as fuel. It was found that the use of a chemically mixed OC had a negative effect on the combustion efficiency since the formation of Fe-Ni compounds reduced the catalytic effect of Ni addition. On the other hand, a physically mixed OC with 2% of NiO increased significantly the combustion efficiency at low temperatures. Whereas, the Fe-Ni-based OCs were only tested for gas combustion in a CLC process, the productions of which were CO₂ and H₂O, the capacity of the Ni active sites to catalyze the chemical looping reforming (CLR) of methane was not investigated, the production of which was synthesis gas rather than heat. Furthermore, though the oxygen carriers' reactivity with different fuel gases in TGA was tested in their work, the multicycle redox reactivity of the Fe-Ni oxygen carrier needed to be further studied.

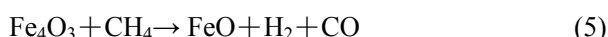
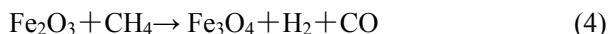
The aim of the current study is to investigate the redox reactivity of Fe₂O₃/Al₂O₃ oxygen carriers modified by low contents of nickel and the reactions occurring between the oxygen carriers and CH₄ in chemical looping reforming process.

In the present work, the Fe₂O₃/Al₂O₃ oxygen carrier was prepared by mechanical mixing method and then it was modified by doping low content nickel to investigate the synergic effect between NiO and Fe₂O₃ or Al₂O₃. Oxygen carriers were exposed alternately to an atmosphere of CH₄ and air to investigate their reactivity when used in the CLR and a series of characterization analyses such as X-ray diffraction (XRD), X-ray fluorescence (XRF), scanning electron microscopy (SEM),

and temperature programmed reduction (TPR) were employed to study the behavior of oxygen carriers before and after cyclic reactions.

Thermodynamics analysis

Thermodynamics analysis of CLR is important for understanding of the reaction mechanism, technical parameters as well as the product composition. Also, it would be useful to know the final state of the oxygen carrier in this work. There are different Fe phases at the oxygen carriers used in this work from the CLR of CH₄, shown as follows:



With related thermodynamic parameters, the equilibrium constants K can be calculated for oxygen carriers with CH₄ in a wide range of operating temperatures. Figure 2 indicates the logarithm of equilibrium constant K as a function of temperature for CLR of CH₄ with the oxygen carriers. It is observed that all the four CLR reaction equilibrium constants increase with the temperature increasing in the range of 600–1200 °C, indicating that the CLR reactions can be enhanced by increasing temperature and the temperature range of 800–900 °C can be suitable for the CLR. Besides, the logarithm of equilibrium constant K for the reaction of Fe₂O₃-Fe₃O₄ varies from 5 to 10, which is the biggest in the four reactions. While, being smaller than the reaction of Fe₂O₃-Fe₃O₄, the lg K for NiO-Ni is about 2–5 and lg K for Fe₃O₄-FeO as well as FeO-Fe are almost less than 4. It is apparent that Fe₂O₃-Fe₃O₄ has a greater tendency to react with CH₄ as compared to Fe₃O₄-FeO and FeO-Fe in the temperature range of 600–1200 °C.

Furthermore, the process of CLR between the oxygen carriers and CH₄ could be accompanied by side reactions like the CLC reaction, thermal pyrolysis, dry

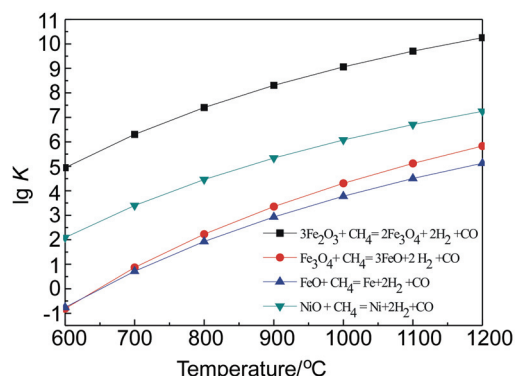


Figure 2 The equilibrium constants for CLR of CH₄ with oxygen carriers.

reforming, steam reforming of CH₄, etc. An acceptable way is to control the stoichiometric ratio of CH₄ and the oxygen carriers to mainly generate the synthesis gas and avoid the side reactions. Also, the productions of CH₄'s dry reforming and CH₄'s steam reforming were H₂ and CO making positive effect on the synthesis gas from CLR, which can be treated as continuation of the reactions between CH₄ and oxygen carriers.

Experimental

Preparation of the oxygen carrier

The Fe₂O₃/Al₂O₃ oxygen carrier with a mass ratio of Fe₂O₃/Al₂O₃=7/3 was prepared by mechanical mixing method and calcination. Starting materials Fe₂O₃ (analytically pure) and Al₂O₃ (analytically pure) were mixed according to the mass ratio, blended in a Planetary Mixer sufficiently and pressed into a 1 mm diameter cylindrical bar by the screw extrusion machine. The resulting mixture was dried at 105 °C for 24 h after natural drying overnight and then calcined at 1100 °C for 6 h in a muffle furnace. Then the fresh oxygen carrier particles (OC1) with size of 60–80 mesh were obtained after grinding and screening. The particles were impregnated respectively in 0.92 mol/L (10%, wt), 2.075 mol/L (20%, wt) and 3.55 mol/L (30%, wt) nickel nitrate solution for 24 h. Then, the sample was dried at 70 °C for 24 h after natural drying overnight and then calcined at 850 °C for 6 h in the muffle furnace and the Fe₂O₃/Al₂O₃ oxygen carrier samples modified with nickel, which were defined as OC2, OC3 and OC4, respectively, were obtained.

Characterization of oxygen carrier

Powder X-ray diffraction (XRD, X'Pert PRO MPD) using Cu K α (40 kV, 40 mA) was used to analyze the crystal structure of fresh and reacted samples. Data was collected between $2\theta=10^\circ-80^\circ$. The element contents in the samples were determined by X-ray fluorescence (XRF, AXIOSMAX-PETRO). Temperature programmed reduction (TPR) experiments were performed on TPR (Quantachrome, CPB-1) under a flow of 5 vol% H₂/He (120 mL/min) with 150 mg oxygen carrier using a heating rate of 10 °C/min. The surface morphology and characteristics of the samples were performed by scanning electron microscopy (SEM) on a Hitachi S4800 instruments. The BET surface was determined by N₂ physisorption using a Micromeritics ASAP 2010 instruments. The samples were degassed under vacuum at 493 K for 6 h before measurement.

Oxygen carrier reactivity test

To test the reduction-oxidation (redox) reactivity, redox multicycle of the oxygen carriers were carried out in a TGA reactor (NETZSCH, STA409C/PC), which is schematically shown in Figure 3. An amount of 15 mg of oxygen carrier was placed in TG reactor. Prior to redox reactions, the oxygen carrier was heated to 850 °C

under atmosphere of pure N₂ at a rate of 10 °C/min. CH₄ (40 vol% CH₄ in N₂) and air were alternately introduced into TG reactor, which is simulating the cyclic conditions of CLR system. To avoid air and methane mixing during the shift between the reduction and oxidation periods, N₂ gas was introduced for 10 min after each period. The total gas flow rate of the reaction was controlled by a mass flow controller at specific flow rate of 20 mL/min (room conditions).

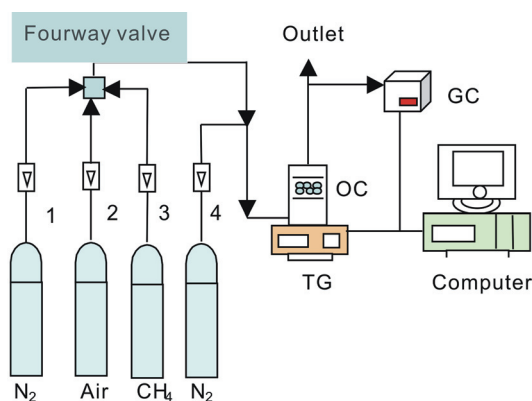


Figure 3 Schematic diagram of oxygen carrier redox experiment device.

Isothermal reaction tests

Isothermal reaction tests were conducted in a fixed bed coupled with a gas chromatograph at 850 °C. An amount of 2 g of oxygen carrier was placed in the reactor and the fixed bed was electrically heated by an oven with a heating rate of 20 °C/min in an inert atmosphere of N₂. After reaching the set temperature, CH₄ (40 vol% CH₄ in N₂) was introduced into the fixed reactor to react with oxygen carriers, the total gas flow rate of the reaction was controlled by a mass flow controller at specific flow rate of 40 mL/min (room conditions). Outlet gas out of the fixed bed was collected with gas bags and analyzed by gas chromatograph (Shimadzu GC-2010 plus). Nitrogen was employed as a carrier gas. CH₄ conversion and H₂/CO molar ratio were calculated based on the analysis results of GC according to the following equation:

$$\text{Methane conversion} = \frac{\text{molar flow of methane consumed}}{\text{molar flow of methane introduced}} \times 100\% \quad (8)$$

$$\text{H}_2/\text{CO molar ratio} = \frac{\text{molar flow of H}_2 \text{ produced}}{\text{molar flow of CO produced}} \times 100\% \quad (9)$$

Results and Discussion

Oxygen carrier characterization

X-ray fluorescence (XRF) Based on the X-ray

fluorescence (XRF) measurement as shown in Table 1, the content of nickel in the different oxygen carrier samples (OC2, OC3, OC4) increased from 0.43 wt% to 1.72 wt% with the concentration of the nickel nitrate solution increased and the samples were composed of over 30 wt% Fe element as reactivity component and over 28 wt% Al element as inert support. Some trace elements including P, Ti, Si, Ca, Cu, *etc.* were simultaneously detected by the XRF measurement, which could be from the preparation process and the film of plastic. On account of trace content, these elements had little influence on the chemical looping reforming of CH₄.

Table 1 XRF analysis results of oxygen carriers modified by nickel

Compound	Sample OC2		Sample OC3		Sample OC4	
	Conc./wt%	Absolute error	Conc./wt%	Absolute Error	Conc./wt%	Absolute error
O	39.55	0.2	39.72	0.3	39.72	0.3
Fe	30.49	0.2	28.87	0.1	28.26	0.1
Al	28.72	0.02	29.58	0.02	29.40	0.04
Ni	0.43	0.02	1.04	0.03	1.72	0.04
P	0.32	0.02	0.26	0.02	0.39	0.03
Ti	0.16	0.01	0.17	0.01	0.19	0.02
Si	0.16	0.02	0.14	0.02	0.14	0.02
Ca	0.09	0.01	0.12	0.01	0.12	0.01
Cu	0.02	0.004	0.01	0.003	0.02	0.004

X-ray diffraction (XRD) The fresh and Ni-modified oxygen carriers were examined by XRD to identify the crystalline phases (Figure 4). It is observed that there are Fe₂O₃ and Al₂O₃ characteristic peaks in the XRD patterns of the original oxygen carrier (OC1), which are in good agreement with JCPDS card 01-089-8104, indicating that the physical properties of Fe₂O₃ did not change during the original preparation process. Meanwhile, the characteristic peaks of NiO (JCPDS 01-089-7390) were detected in the samples of OC2, OC3 and OC4, which indicated that the Ni(NO₃)₂ was decomposed into NiO in the preparation process. Also, it is noted that NiFe₂O₄, NiAl₂O₄ crystalline phases were detected in the modified samples OC3 and OC4 respectively (JCPDS 00-003-0875, 01-071-0965). There were four crystalline phases in OC3 and four in OC4, which demonstrated the synergistic effect between Fe₃O₄, Al₂O₃ and NiO.^[33,34] It was suggested that reaction between NiO and Fe₂O₃ occurs to generate NiFe₂O₄ during calcination process. Besides, NiO may react with Al₂O₃ to produce NiAl₂O₄ with the increase of nickel content in the oxygen carriers, however, both the NiFe₂O₄ and NiAl₂O₄ were not detected in the sample of OC2 for the reason that the nickel content was too little to be detected by the XRD.

The XRD patterns of the oxygen carriers reoxidized after redox cyclic reactions are shown in Figure 5. It was

observed that the original and Ni-modified samples kept the main phase structure although Fe_3O_4 was detected (ICPS 01-088-0315), suggesting the samples in a good crystalline state after successive cyclic redox reactions and partial oxygen carriers were not oxidized completely. The XRD patterns indicate that the synthetic oxygen carriers have good regenerability and reactivity.

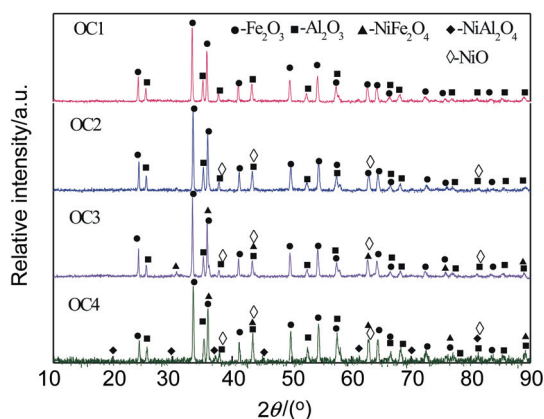


Figure 4 XRD patterns of fresh oxygen carriers.

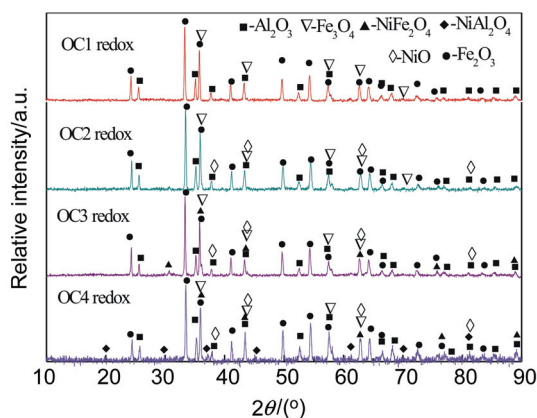


Figure 5 XRD patterns of reoxidized oxygen carriers after redox cyclic reactions.

Temperature-programmed reduction (TPR)

TPR was performed aiming to investigate the reducibility of the prepared oxygen carriers. As shown in Figure 6, it is clear that there are three reduction peaks in the TPR profiles of the OC1, which are observed at the temperature of 440, 611, and 673 °C.^[39,40] Similarly, the TPR profiles for the sample OC2 present three stronger peaks in the temperature range from 430 to 750 °C without a defined maximum. Whereas, the TPR profiles for the rest samples OC3, OC4 show a reduction peak at about 340–355 °C and other peaks at 500–950 °C. It was reported that the generated sequence of reduction products of Fe_2O_3 was Fe_3O_4 , FeO , and Fe .^[41,42] Therefore, we can infer that the first reduction peak of OC1 at 440 °C was attributed to the transformation of Fe_2O_3 to Fe_3O_4 via reacting with H_2 . Also, the rest two peaks at the temperature 611, 673 °C were assigned to FeO and Fe , which came from the further reduction of

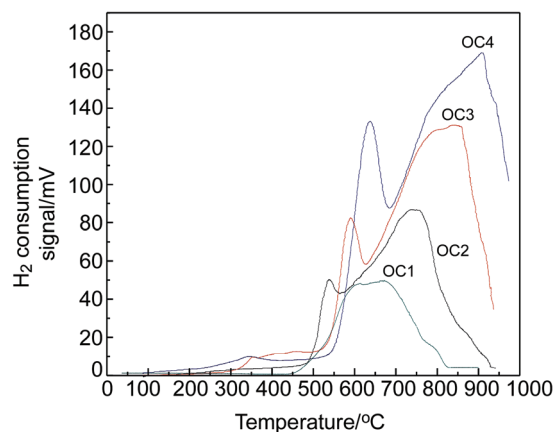
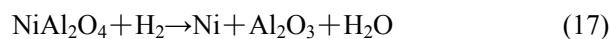
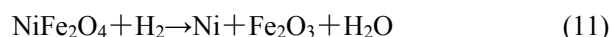


Figure 6 H_2 -TPR analysis of original OC & modified samples.

Fe_3O_4 by reacting with H_2 . On the basis of the TPR curves, it is observed that the unmodified OC1 can provide lattice oxygen for the reaction of CLR of methane. However, it requires higher activation energy in deeper reduction stage in comparison to the nickel modified oxygen carriers. As an inert support, Al_2O_3 can be used to enhance the strength, improve specific surface area and anti-sintering of the oxygen carrier without reacting with H_2 .

In comparison to OC1, the TPR profile for the sample OC2 displayed slight shift to lower temperature for the first peak and higher temperature for the second peak, which can be explained by the reduction of NiO highly dispersed on pores of $\text{Fe}_2\text{O}_3/\text{Al}_2\text{O}_3$ samples.

While, the rest two samples OC3, OC4 showed a modest reduction peak at the defined temperature 350 °C followed by two intense H_2 consumption peaks at about 580–900 °C for each sample, which can be illustrated by NiFe_2O_4 , NiAl_2O_4 identified by XRD and reacted by the following Eq.^[43-45]



Generally, the first reduction peak at 350 °C was primarily attributed to the reduction of crystal NiO whose quantity was too little to be detected in the samples. Besides the formation of Fe_3O_4 and FeO , the second and third H_2 consumption peaks are associated with the reduction of NiFe_2O_4 and NiAl_2O_4 as shown in equations 11, 12, 13, 14 and 17. Also, the second and

third H₂ consumption peaks exhibit features similar to those of peaks increasing in intensity and shifting to higher temperatures with increasing content of nickel. It can be explained by that more amounts nickel oxide and Fe-Ni alloy generated in the later stage reaction, which limited H₂ to permeate the pores of the particles.^[46]

It was clear that a little added nickel (less than 0.5 wt%) can improve the reactivity of the oxygen carrier and with the content of nickel increasing, NiFe₂O₄, NiAl₂O₄ generated sequentially as well as Fe-Ni alloy in the oxygen carriers (detected by XRD, JCPDS 03-065-7752), which were shown at corresponding reduction peaks in TPR.

Successive redox cycles reactivity

To test successive redox reactivity of the nickel decorated samples, multicycles of redox of the oxygen carriers exposed to alternating methane and air conditions were carried out in the TGA reactor at 850 °C. In present work, each sample was tested for 20 cycles. As a result, different reactivity was observed during the experiments for the four kinds of oxygen carriers with various contents of nickel. The mass change which reflected the degree of oxidation or reduction, as a function of time for each sample is shown in Figure 7. As for the sample OC1, there was approximately 4% mass loss when the samples were exposed in CH₄ flow, which indicates 19 wt% reactive lattice oxygen in the OC1 was used as oxidant ($m_{\text{Fe}_2\text{O}_3} : m_{\text{Al}_2\text{O}_3} = 7 : 3$). If the samples were further reduced from the mass 94.5 wt% to less,

the reaction rate became much slower. Therefore, when the consumption of lattice oxygen in the OC1 was close to 19 wt%, the atmosphere was shifted from methane to air to regenerate the oxygen carrier. The oxidation rates of reduced samples in air flow were quite faster in comparison to their reduction stage. As the number of redox cycles increased, the reaction rate and weight loss ratio began to decrease for the reason of sintering.

In comparison to the original OC1, the samples OC2 gave a relatively bigger degree of reduction changes, with weight loss up to 81% in the reduction stage [Figure 7(b)]. Meanwhile, the slope of mass loss curve increases, which indicated that the redox rate was improved greatly. As for the samples OC3, OC4, the changes of weight loss ratio during the methane oxidations are very close to the samples OC2, while, giving higher reaction rates than it. Though the two samples OC3, OC4 showed a close reaction rate, the rate of carbon deposition on the two oxygen carriers was different. It was found that OC4 caused more carbon deposition in the later stage of methane oxidation.

In brief, as the reaction time is prolonged, the original OC1 is prone to sintering to lead to decline in reactivity, while low content nickel decorated samples can display better reactivity in reduction stage and better regenerability in oxidation stage. The redox reaction rate and weight loss rate of the nickel modified samples were improved significantly, however, more carbon deposition was observed on the samples with more nickel content in the course of redox cycles, which was

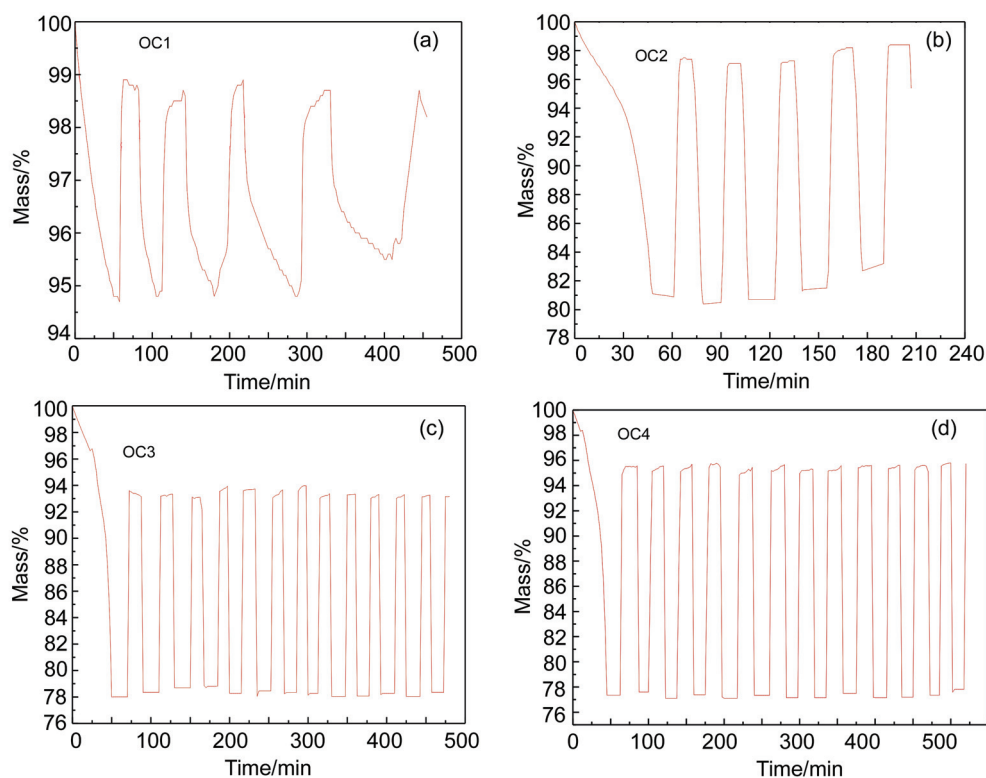


Figure 7 Mass changes of oxygen carriers with reaction time in successive redox cycles. (a) Mass changes of OC1, (b) mass changes of OC2, (c) mass changes of OC 3, (d) mass changes of OC4.

from 11.4 wt% of OC2 to 13.1 wt% of OC3 and 17.9 wt% of OC4. The reactivity was not much improved in redox rate as the content of nickel increased in the samples when it was more than 1 wt%, which was in agreement with the open literatures.^[31] Therefore, the content 1.04 wt% of nickel was the optimum in the three modified samples with integration of reactivity and carbon deposition.

Isothermal reaction tests

Isothermal reaction tests were conducted in a fixed bed coupled with a gas chromatograph at 850 °C. The outlet gas concentrations as a function of time in the course of methane oxidation reactions for the four kinds of the oxygen carriers are shown in Figure 8. Figure 9 illustrates typical kinetic curves of methane conversion and H₂/CO ratio towards the reaction of methane with oxygen carriers. The four kinds of oxygen carriers give high methane conversion at the initial stage and OC4 presents the highest methane conversion. Afterward, there is a sharp decline of methane conversion from 1 to 12 min, then a quick increase thereafter for the OC1, OC2 and OC3. On the other hand, the OC4 displays a different variation trend, which gives a steady state level over 95 wt% of the methane conversion till 25 min and then declines dramatically. The initial decline of methane conversion could be attributed to the high consumption rate of surface absorption oxygen, while bulk lattice oxygen in oxygen carrier can not be released as soon as possible to supplement this deficiency. As seen in Figure 8, the reaction initially occurs to generate high concentrations of CO₂ with little fractions of CO and H₂ in the early stage. As the reaction proceeds, the CO₂ fractions decrease sharply after 15th minute, whereas the CO fractions increase continuously and then keep stable. Apparently, CH₄ is mainly oxidized to CO₂ and H₂O in total oxidation at the beginning of the reaction, then is partially oxidized to H₂ and CO in the mid and later stages, which can be verified by the H₂/CO ratio as shown in Figure 9 as well. As above mentioned, the oxygen species is classified into two types: surface absorbed oxygen and bulk lattice oxygen. Surface oxygen contributes to the complete oxidation of methane to CO₂ and H₂O, because it has high reactivity. The lattice oxygen is usually prone to CH₄ partial oxidation into H₂ and CO. It is clear that the higher degree of methane deep oxidation at the early stage is due to the surface oxygen species on the fresh oxygen carrier particles. As the surface oxygen species is depleted, lattice oxygen diffused from the bulk to surface of particles to cause the methane selective oxidation resulting in the increase of the CO and H₂ fractions. This is easy to explain why methane is oxidized to CO₂ and H₂O at the initial stage of the reaction and then selectively oxidized to CO and H₂ at later stage. Literatures gave very similar results to this work.^[47]

For the samples of OC1 and OC2, the fractions of H₂ and CO are lower than CO₂ even in the initial stage. As

the reaction proceeded, the fractions of CO₂ reversed at 20th minute, the fractions of CO and H₂ increased quickly (Figures 8a and 8b). The methane conversion of the two samples was lower and the original OC1 gave the lowest methane conversion rate among the four oxygen carriers (Figures 9a, 9b). A reason was that the diffusivity of lattice oxygen from NiO and NiFe₂O₄ can reduce the activation energy and enhance the reactivity of the oxygen carrier,^[34] which was also demonstrated by TPR measurement as shown in Figure 6. Also, the H₂/CO ratio was near to 2, suggesting more methane was partial oxidized to CO and H₂. With low content nickel, the samples of OC2 exhibited very similar profiles of gas distribution versus reaction time, but a higher methane conversion rate than original samples.

The samples of OC3 and OC4 displayed higher methane conversion and H₂ concentration, moreover, the later gave the highest methane conversion rate among the four samples. From Figure 8 c and d, it can be seen that H₂ is the overwhelming gas product during the whole reaction process and the CO/H₂ ratio increases rapidly after the reaction time of 25 min, reaching 20 at 35 min. This indicates that methane starts to decompose to H₂ and carbon in the later stage of the reaction. Furthermore, as the surface oxygen is consumed, the increasing concentration of lattice oxygen vacancies may provide pathways of oxygen transport through the lattice, therefore, it is rather reasonable that the methane conversion rose rapidly with the reducing of surface NiFe₂O₄ or other oxygen species after the reaction time of 12 min and declined with the lattice oxygen depletion. An exception was the sample OC4, the methane conversion curves kept stable in a range from beginning to 25 min, which can be attributed to the NiAl₂O₄ to improve reaction activity of lattice oxygen in the oxygen carrier with the proper content.

Though lattice oxygen from nickel oxide can enhance the reactivity of the oxygen carrier, more content of nickel is prone to generate methane decomposition, which is a negative factor for the chemical looping reforming (CLR).

SEM micrographs

The shape and morphological features of the fresh and used iron based oxygen carriers at 850 °C were characterized by SEM and the result was shown in Figure 10. It is observed that the four kinds of fresh oxides have similar micro morphology, which are in good agreement with the oxygen carriers synthesized by combustion and deposition-precipitation method reported by previous literatures.^[48] The morphology of the fresh oxygen carriers particles exhibits irregular cube structure with an average size of around 3–6 μm. Particles of Al₂O₃, NiFe₂O₄ and NiAl₂O₄ were dispersed on that of Fe₂O₃. Small interconnected pores exist on the surface of particles, which are beneficial to diffusion and penetration of reactant gas in to solid particles. When the samples were exposed to successive alternat-

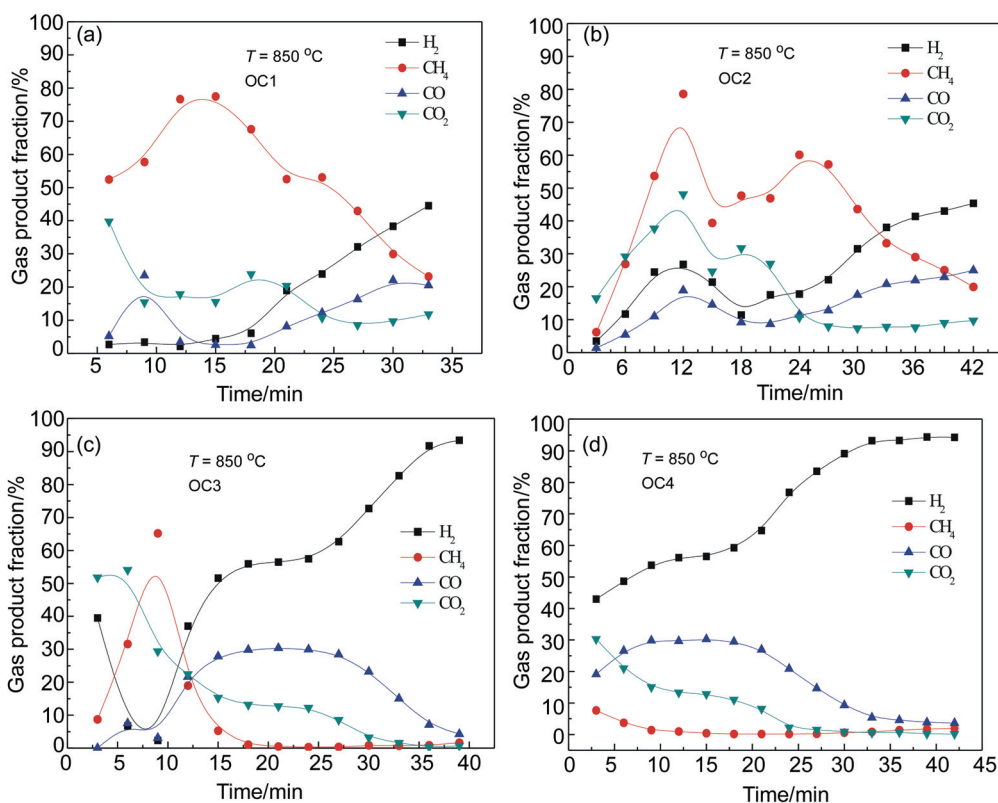


Figure 8 Gas concentration profiles of methane chemical looping reforming by using different oxygen carriers. (a) OC1, (b) OC2, (c) OC3, (d) OC4.

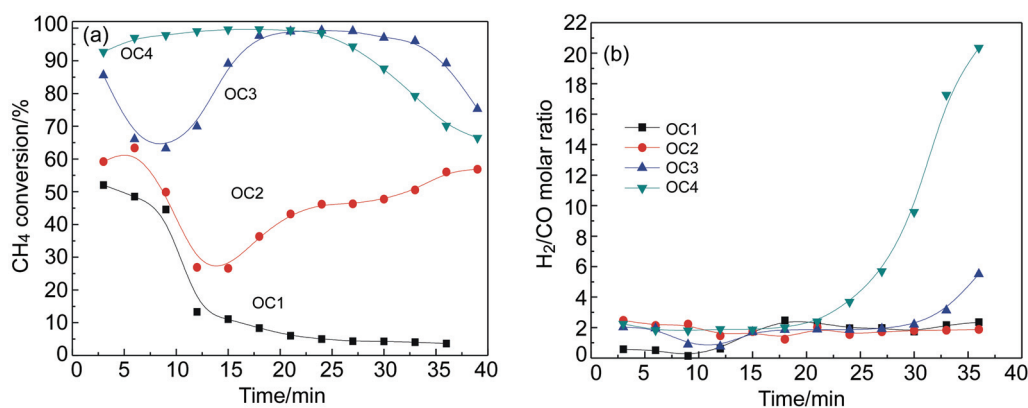


Figure 9 Methane conversion (a) and H₂/CO molar ratio (b) as a function of time during methane oxidation reactions.

ing reducing and oxidizing atmosphere, sintering occurred in OC1 particles and the particles were agglomerated into the massive structure, while, though agglomeration occurred in OC2 and OC3 samples, serious sintering did not happen and the particle size decreased indicating that the NiFe₂O₄ can prevent sintering and improve redox reactivity (shown in Figures 10d, 10f, 10h). OC4 maintained the crystalline phase structures after 20 cycles, though the surface became much rougher and the irregular cube was loosened in the course of cyclic reactions.

Specific surface area analysis

Table 2 lists the BET-surface area of the synthesized

oxygen carriers fresh and after redox cyclic reactions. It is observed that the surface area decreases with the content of nickel in the oxygen carrier samples increasing, which indicates that the NiFe₂O₄, NiAl₂O₄, particles disperse into the pores of Fe₂O₃/Al₂O₃ in the process of preparation. Therefore, the improvement in oxygen carrier by performance based nickel addition can be ascribed to a mechanism of chemical effect like NiFe₂O₄

Table 2 Specific surface area of the synthesized oxygen carriers

Fe-based oxygen carrier	OC1	OC2	OC3	OC4
BET surface area/ (m ² ·g ⁻¹)				
Fresh	3.194	3.057	3.028	2.544
Regenerated	1.299	2.712	2.703	2.767

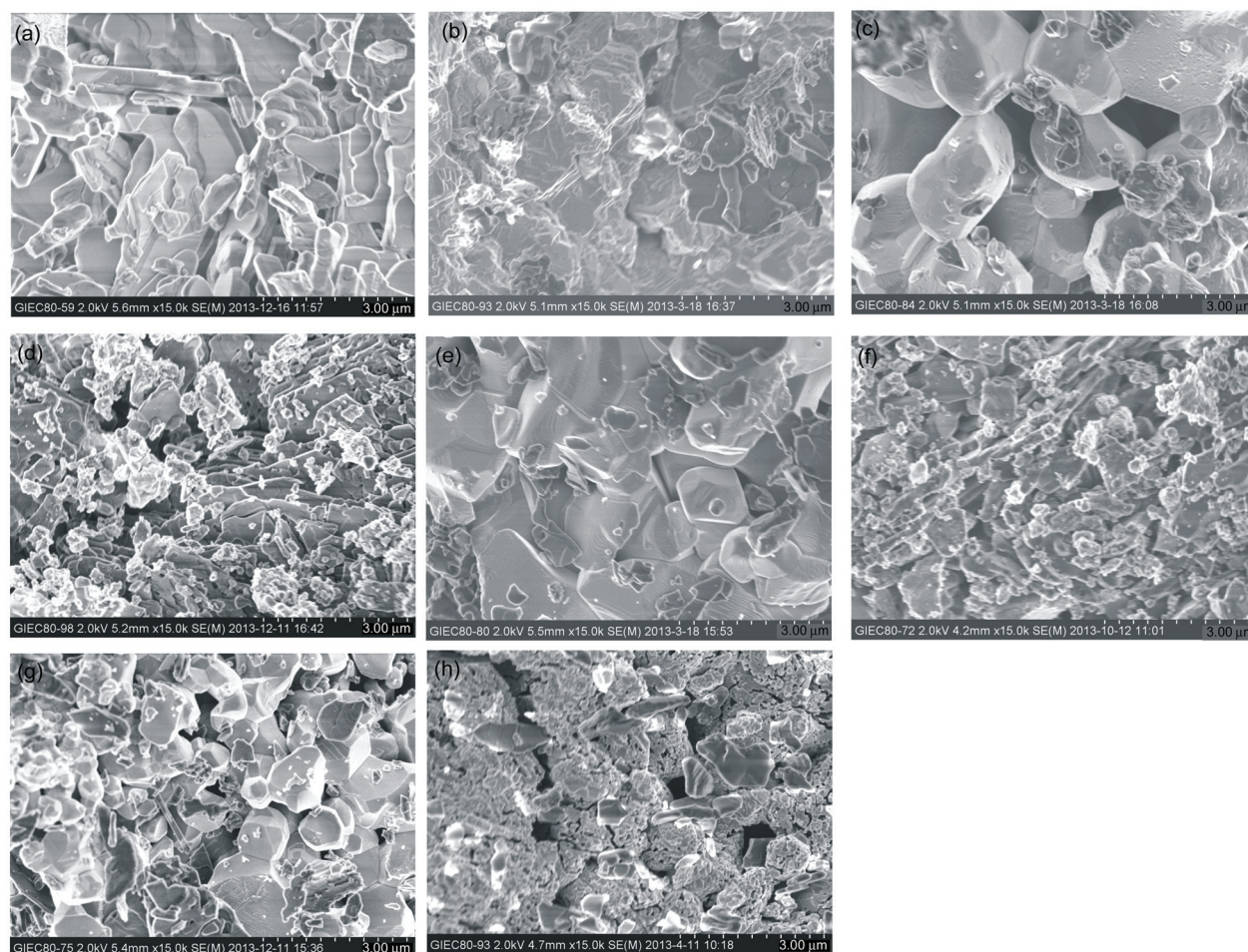


Figure 10 SEM analysis of fresh and decorated oxygen carriers by nickel before and after redox cyclic reactions. (a) OC1 fresh, (b) OC1 after redox reactions, (c) OC2 fresh, (d) OC2 after redox reactions, (e) OC3 fresh, (f) OC3 after redox reactions, (g) OC4 fresh, (h) OC4 after redox reactions.

other than surface area enhancement. Furthermore, the specific surface areas of the former three samples decrease after redox cycles and that of OC1 declines rapidly leading to decrease of the reaction activity, which could be ascribed to thermal sintering and agglomeration occurred in the oxygen carrier particles. However, the surface of OC4 slightly increases after 20 times cyclic reactions, this can be illustrated by the crack and interstice of oxygen carrier particles in the process of lattice oxygen release and recover, which can be obviously confirmed by the SEM images of Figure 10. Also, the reactivity of the decorated sample did not decline significantly, which was identified by XRD patterns (Figure 5) and mass changes with reaction time (Figure 7). As the NiFe_2O_4 , NiAl_2O_4 generating, the reactivity and anti-sintering of the oxygen carriers particles were improved in different degrees.^[49] The resistance to sintering of the modified samples increased with the NiO addition increasing.

Conclusions

In the present research, $\text{Fe}_2\text{O}_3/\text{Al}_2\text{O}_3$ oxygen carriers

with low content of nickel for chemical-looping reforming of methane were prepared by mechanical mixing and impregnation method. XRF, XRD and TPR results indicated that the $\text{Fe}_2\text{O}_3/\text{Al}_2\text{O}_3$ oxygen carriers have good regenerability and NiO particles can create synergic effect with the $\text{Fe}_2\text{O}_3/\text{Al}_2\text{O}_3$ particles to generate NiFe_2O_4 and NiAl_2O_4 spine phases. Also, the cyclic reactivity test in TGA showed that low content nickel addition may improve the reactivity of the oxygen carriers, however, the improvements were not apparent as the content of nickel increased to more than 1 wt% in the samples due to the methane decomposition and carbon deposition. Besides, the isothermal reaction tests in fixed bed displayed that the surface absorbed oxygen contributed to oxidizing methane completely to CO_2 and H_2O in the initial stage of the reaction, whereas the bulk lattice oxygen prone to methane partial oxidation into H_2 and CO. The SEM and BET analysis confirmed that NiFe_2O_4 , NiAl_2O_4 particles disperse into the porosity of $\text{Fe}_2\text{O}_3/\text{Al}_2\text{O}_3$ particles in the process of preparation. In addition, the anti-sintering of the oxygen carriers particles was increased with the NiO addition increasing. Consequently, the content of nickel doping

in the oxygen carrier from 0.43 wt% to 1.72 wt% was investigated for CLR of methane, the content 1.04 wt% of nickel doping was optimal in the three modified samples with integration of reactivity and carbon deposition.

Acknowledgement

The financial support of the National Natural Science Foundation of China (No. 51076154) is gratefully acknowledged. This work was also supported by the National Key Technology R&D Program of 12th Five-Year Plan of China (No. 2011BAD15B05) and the Science & Technology Research Project of Guangdong Province (No. 2010B010900047).

References

- [1] He, F.; Wei, Y.-G.; Li, H.-B.; Wang, H. *Energy Fuels* **2009**, *23*, 2095.
- [2] Chen, P.; Hou, Z.-Y.; Zheng, X.-M. *Chin. J. Chem.* **2005**, *23*, 847.
- [3] Dai, X.-P.; Yu, C.-C.; Li, R.-J.; Wu, Q.; Hao, Z.-P. *J. Rare Earths* **2008**, *26*, 76.
- [4] Wei, Y.; Wang, H.; He, F.; Ao, X.-Q.; Zhang, C.-Y. *J. Nat. Gas Chem.* **2007**, *16*, 6.
- [5] Gnanapragasam, N. V.; Reddy, B. V.; Rosen, M. A. *Int. J. Hydrogen Energy* **2010**, *35*, 4788.
- [6] Mendiara, T.; Jensen, A.; Glarborg, P. In *Chemical Looping Reforming of Generator Gas*, Technical University of Denmark, Department of Chemical and Biochemical Engineering, Kongens Lyngby (DK), Copenhagen, **2010**, p. 145.
- [7] Copeland, R. J.; Alptekin, G.; Cesario, M.; Gershanovich, Y. In *Proceedings of the 27th International Technical Conference on Coal Utilization & Fuel Systems*, Clearwater, Vol. 2, Florida, March 4–7, **2002**, pp. 719–729.
- [8] Cho, P.; Mattisson, T.; Lyngfelt, A. *Fuel* **2004**, *83*, 1215.
- [9] Forutan, H. R.; Karimi, E.; Hafizi, A.; Rahimpour, M. R.; Keshavarz, P. *J. Ind. Eng. Chem.* **2014**, DOI: 10.1016/j.jiec.2014.04.031.
- [10] Anders, L.; Bo, L.; Tobias, M. *Chem. Eng. Sci.* **2001**, *56*, 3101.
- [11] Mihai, O.; Chen, D.; Holmen, A. *Ind. Eng. Chem. Res.* **2011**, *50*, 2613.
- [12] Fossdal, A.; Bakken, E.; Øye, B. A.; Schøning, C.; Kaus, I.; Morkelbost, T.; Larring, L. *Int. J. Greenh Gas Con.* **2011**, *5*, 483.
- [13] Abad, A.; Adánez, J.; Francisco, G. L.; de Diego, L. F.; Pilar, G. *Combust. Flame* **2010**, *157*, 602.
- [14] Iñaki, A. R.; Arjmand, M.; Leion, H.; Pilar, G.; Abad, A.; Mattisson, T.; Lyngfelt, A. *Energy Fuels* **2013**, *27*, 3918.
- [15] Shen, L.-H.; Wu, J.-H.; Gao, Z.-P.; Xiao, J. *Combust. Flame* **2010**, *157*, 934.
- [16] Jerndal, E.; Mattisson, T.; Thijs, I.; Snijkers, F.; Lyngfelt, A. *Int. J. Greenh Gas Con.* **2010**, *4*, 23.
- [17] Moldenhauer, P.; Rydén, M.; Mattisson, T.; Lyngfelt, A. *Fuel Process. Technol.* **2012**, *104*, 378.
- [18] Arjmand, M. L.; Mattisson, T.; Lyngfelt, A. *Int. J. Greenh Gas Con.* **2014**, *22*, 154.
- [19] Ksepko, E.; Sciazko, M.; Babinski, P. *Appl. Energy* **2014**, *115*, 374.
- [20] Wang, B.-W.; Zhao, H.-B.; Zheng, Y.; Liu, Z.-H.; Rong, Y.; Zheng, C.-G. *Fuel Process. Technol.* **2012**, *96*, 104.
- [21] Wang, B.-W.; Rong, Y.; Lee, D.-H.; Zheng, Y.; Zhao, H.-B.; Zheng, C.-G. *J. Anal. Appl. Pyrol.* **2011**, *91*, 105.
- [22] Adanez, J.; Abad, A.; Francisco, G. L.; Pilar, G.; de Diego, L. F. *Prog. Energy Combust. Sci.* **2012**, *38*, 215.
- [23] Gu, H.-M.; Shen, L.-H.; Xiao, J.; Zhang, S.-W.; Song, T.; Chen, D. *Combust. Flame* **2012**, *159*, 2480.
- [24] Pans, M. A.; Gayán, P.; Abad, A.; Francisco, G. L.; de Diego, L. F.; Adánez, J. *Fuel Process. Technol.* **2013**, *115*, 152.
- [25] Bhavsar, S.; Vesper, G. *Ind. Eng. Chem. Res.* **2013**, *52*, 15342.
- [26] He, F.; Galinsky, N.; Li, F.-X. *Int. J. Hydrogen Energy* **2013**, *38*, 7839.
- [27] Li, K.-Z.; Wang, H.; Wei, Y.-G.; Yan, D.-X. *Biochem. Eng. J.* **2010**, *156*, 512.
- [28] Zhu, J.-H.; Geng, S.-J.; Ballard, D. A. *Int. J. Hydrogen Energy* **2007**, *32*, 3682.
- [29] Pour, N.-M.; Leion, H.; Rydén, M.; Mattisson, T. *Energy Fuels* **2013**, *27*, 6031.
- [30] Rydén, M.; Leion, H.; Mattisson, T.; Lyngfelt, A. *Appl. Energy* **2014**, *113*, 1924.
- [31] Rydén, M.; Lyngfelt, A.; Mattisson, T.; Chen, D.; Holmen, A.; Bjørgum, E. *Int. J. Greenh Gas Con.* **2008**, *2*, 21.
- [32] Nalbantian, L.; Evdou, A.; Zaspalis, V. *Int. J. Hydrogen Energy* **2011**, *36*, 6657.
- [33] He, F.; Li, X.-A.; Zhao, K.; Huang, Z.; Wei, G.-Q.; Li, H.-B. *Fuel* **2013**, *108*, 465.
- [34] Geng, S.-J.; Li, Y.-D.; Ma, Z.-H.; Wang, L.-L.; Li, L.-N.; Wang, F.-H. *J. Power Sources* **2010**, *195*, 3256.
- [35] Chen, D.-Q.; Shen, L.-H.; Xiao, J.; Song, T.; Gu, H.-M.; Zhang, S.-W. *J. Fuel Chem. Technol.* **2012**, *40*, 267.
- [36] Kim, K.; Yang, S.; Baek, J. I.; Ryu, C. K.; Choi, M.; He, Y. S.; Shin, K.; Lee, G. *Fuel* **2013**, *111*, 496.
- [37] Bermúdez, J. M.; Fidalgo, B.; Arenillas, A.; Menéndez, J. A. *Fuel* **2012**, *94*, 197.
- [38] Benrabaa, R.; Boukhlof, H.; Löfberg, A.; Rubbens, A.; Bordes-Richard, E.; Vannier, R. N.; Barama, A. *J. Nat. Gas Chem.* **2012**, *21*, 595.
- [39] Kobayashi, Y.; Horiguchi, J.; Kobayashi, S.; Yamazaki, Y.; Omata, K.; Nagao, D.; Konnob, M.; Yamada, M. *Appl. Catal.* **2011**, *395*, 129.
- [40] Gobara, H. M. *Egypt J. Petroleum* **2012**, *21*, 1.
- [41] Zhang, Y.-X.; Doroodchi, E.; Moghtaderi, B. *Appl. Energy* **2014**, *113*, 1916.
- [42] Benrabaa, R.; Löfberg, A.; Rubbens, A.; Bordes-Richard, E.; Vannier, R. N.; Barama, A. *Catal. Today* **2013**, *203*, 188.
- [43] Ana, L. G. L.; Aznar, M.; Grasa, G. S.; García, T.; Murillo, R. *J. Power Sources* **2013**, *242*, 371.
- [44] Marrero-Jerez, J.; Chinarro, E.; Moreno, B.; Colomer, M. T.; Jurado, J. R.; Núñez, P. *Ceram. Int.* **2014**, *40*, 3469.
- [45] Hossain, M. M.; Lopez, D.; Herrera, J.; de Lasa, H. I. *Catal. Today* **2009**, *143*, 179.
- [46] Anton, R. *Carbon* **2009**, *47*, 856.
- [47] He, F.; Li, X.-A.; Zhao, K.; Huang, Z.; Wei, G.-Q.; Li, H.-B. *Fuel* **2013**, *108*, 465.
- [48] Gayán, P.; Dueso, C.; Abad, A.; Adanez, J.; de Diego, L. F.; Francisco, G. L. *Fuel* **2009**, *88*, 1016.
- [49] Siew, K. W.; Lee, H. C.; Jolius, G.; Cheng, C. K. *J. Energy Chem.* **2014**, *23*, 15.

(Lu, Y.)